Preprints.org

Symmetry of structures under two-dimensional instability in a finite-height horizontal layer of boiling liquid

Aleksandr N. Pavlenko [*] and Vladimir I. Zhukov

Article

Symmetry of Structures under Two-Dimensional Instability in a Finite-Height Horizontal Layer of Boiling Liquid

Vladimir I. Zhukov [1,2] and Aleksandr N. Pavlenko [1,*]

[1] Kutateladze Instgitute of Thermophysics SB RAS, Novosibirsk, Russia
[2] Novosibirsk State Technical University, Novosibirsk, Russia
* Correspondence: pavl@itp.nsc.ru

Abstract: Two-dimensional instability of a horizontal layer of boiling liquid with a finite height is experimentally studied. In this layer, "vapor columns" rose at the corners of a square rectangular grid. The symmetry of "vapor column" location on the heating surface is considered. The model considers the approach to the boiling crisis in terms of both developed nucleate boiling and transitional boiling (the Zuber problem). When dealing with developed nucleate boiling, the layer of boiling liquid is considered in calculations as an isotropic homogeneous system (foam). It is shown how the conditions on the heating surface (capillary-porous coating) affect external hydrodynamics of the liquid layer and, ultimately, the value of the critical heat flux. The calculation ratio obtained by approaching the boiling crisis with regard to developed nucleate boiling takes into account the dependence of the critical heat flux on the void fraction of the boiling liquid layer. A new solution to the boiling crisis problem is proposed when approaching the crisis from the point of transitional boiling (the Zuber problem). This new solution eliminates some shortcomings of the classical problem (in particular, the void fraction of the layer corresponds to the experiments).

Keywords: horizontal liquid layer; boiling; critical heat flux; instabilities; capillary-porous coating; void fraction

1. Introduction

In 1950 S.S. Kutateladze was the first who substantiated in detail the hydrodynamic (hydromechanical) theory of boiling crisis. In [1], he wrote: "Let us make the following four assumptions.

1. Changes in the boiling regime occur due to a change in the hydrodynamic regime of the two-phase boundary layer that exists during vaporization on the heating surface, and they are characterized by the certain critical values of the vaporization rate.

2. The boundary two-phase layer is so turbulent due to the vaporization process that molecular friction can be neglected both in the vapor and in the liquid flow components.

3. The velocity of a liquid component near the heating surface, due to deceleration created by the latter, is significantly less than the average vapor velocity.

4. The dimensions of the heating surface are so much larger than the bubbles and films freely formed in its immediate vicinity that the occurrence of a crisis in the vaporization regime is equally probable at all points of this surface. "

In [2], he adds the sentence: "The ideal model, which fully satisfies the last condition, is a very large horizontal plate with the heating surface facing upwards."

As a result, using the method of dimensional analysis, Kutateladze obtained the relation for calculating the critical heat flux (CHF) in the process of pool boiling:

$$q_{cr} = k h_{LG} \rho_v \left(\frac{\sigma g (\rho_l - \rho_v)}{\rho_v^2} \right)^{1/4}, \qquad (1)$$

where the value of constant k (called usually the Kutateladze constant) varies within $0.13 - 0.19$; in [1,2] it is recommended to use its average value equal to 0.16; h_{LG} is the latent heat of vaporization; g is the acceleration of gravity; σ is the surface tension coefficient; ρ_l, ρ_v are the densities of liquid and vapor, respectively.

In [3,4], Zuber obtained a formula similar to (1) based on a physical model using the results of the analysis of Taylor and Helmholtz instabilities. **Figure 1** shows the boiling curve from [3], where AB is the convective heat transfer regime, the no-boiling region; BC is the regime of nucleate boiling; CD is the regime of transitional boiling; DE is the film boiling regime; at point C, the boiling crisis begins. In this diagram, the branches BC and CD of the boiling curve in logarithmic coordinates are almost symmetrical relative to the vertical axis drawn through point C.
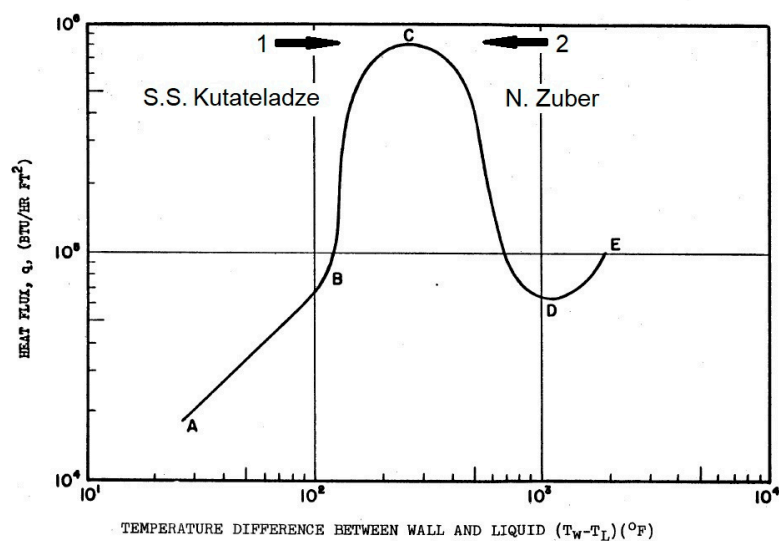

FIGURE I. A TYPICAL CURVE OF HEAT FLUX DENSITY VERSUS SURFACE TEMPERATURE IN BOILING

Figure 1. Boiling curve [3].

It follows from the literature review given in [3] that Zuber was well acquainted with the works of Kutateladze [1,2]. In [3], he writes: "Because the flow configuration in nucleate boiling is not well defined, an analysis of the critical heat flux performed by considering nucleate boiling is reduced to dimensional analysis." Kutateladze in his works [1,2] performed a dimensional analysis and considered the transition to CHF in terms of nucleate boiling (shown by arrow 1 in **Figure 1**).

In his model [3,4], Zuber considered the transition to CHF in terms of transitional boiling (shown by arrow 2 in **Figure 1**). The only quantitative experimental study of transitional boiling in the literature at the time of model development was [5]. The process of methanol boiling on a horizontal copper tube with an outer diameter of 3/8 inch (~9.5 mm) and a working length of about 6 inches (~152 mm) was studied there. The tube was heated with steam. Zuber studied the photographs and description of transitional boiling on the horizontal tube, presented in [5]. Further in [3] he wrote: "… because of Taylor instability, a definite geometrical configuration can be expected in transitional boiling. We shall make use of this defined geometry and analyze, therefore, the critical heat flux by considering transitional boiling", as well as "Thus, in the region of the critical heat flux a small increase of the heat flux density results in a large increase of the surface temperature. Consequently, in the $q = \Delta T$ plane there exists a plateau across which boiling changes from the nucleate to the transitional boiling regime". Based on the analysis of observations on a tube, he formulated the main theoretical provisions for calculating the boiling crisis on an infinite horizontal surface. The Zuber model considers an already formed vapor film on a plane under a liquid layer. Taylor in [6] showed

that the interface separating two liquids of different densities is unstable if the acceleration is directed from a heavier medium to a lighter one. Bellman and Pennington [7] showed that interface perturbations can be stable or unstable depending on whether the critical wavelength is shorter or longer, given by the equation $\lambda_{cr} = 2\pi l_\sigma$, where $l_\sigma = (\sigma / g(\rho_l - \rho_v))^{1/2}$ is the capillary constant. They also showed that the "most dangerous" instability wavelength, i.e., the wavelength at which the perturbation amplitude grows most rapidly, is determined by the expression $\lambda_d = 2\pi\sqrt{3}l_\sigma$. In the Zuber model (**Figure 2**), vapor jets rise up at the vertices of a square grid with a side corresponding to the characteristic Taylor instability wavelengths. The critical vapor velocity in jets is determined by the Helmholtz instability. The wavelength of the Helmholtz instability was taken equal to $\lambda_H = 2\pi R_j$, where $R_j = \lambda_{cr} / 4$ or $R_j = \lambda_d / 4$, where R_j is a vapor jet radius. For the critical heat flux, Zuber obtained the following expression:

$$q_{crZ} = k h_{LG} \rho_v \left(\frac{\sigma g(\rho_l - \rho_v)}{\rho_v^2} \right)^{1/4} \left(\frac{\rho_l}{\rho_l + \rho_v} \right)^{1/2}, \tag{2}$$

where $k_1 = \dfrac{\pi}{24} \dfrac{3}{\sqrt{2\pi}} = 0.157$, if $R_j = \lambda_{cr} / 4$ and $k_2 = \dfrac{\pi}{24} \dfrac{3}{\sqrt{2\pi}} \dfrac{1}{3^{1/4}} = 0.12$, if $R_j = \lambda_d / 4$.

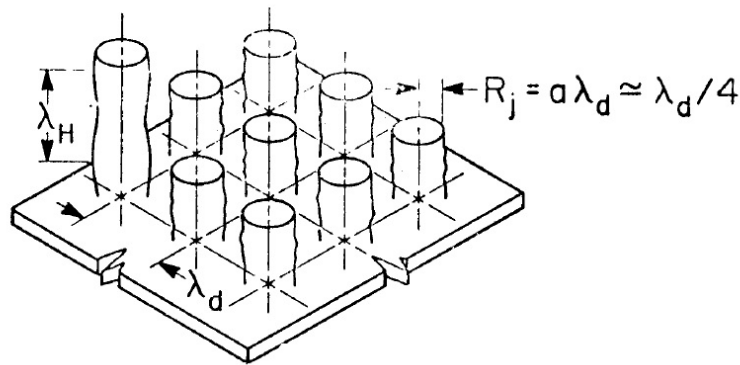Zuber recommends taking $k = \pi/24 = 0.131$ as the most appropriate value.

Figure 2. Schematic diagram of vapor jet location on an infinite horizontal surface according to the Zuber hydrodynamic instability model. The figure is taken from [21].

Authors of [8] proposed to improve the Zuber equation for CHF by assuming $\lambda_H = \lambda_d$ and they obtained $k = 0.149$. In [9], $k = 0.151$ was obtained by considering the interfacial detachment mechanism.

Due to the fact that equations (1) and (2) almost coincide (the expression under the root on the right in formula (2) noticeably differs from one only at near-critical pressures), in some publications one can come across the terms "Kutateladze–Zuber theory" or "Kutateladze–Zuber equation". There is a note on the difference in approach to the boiling crisis in Theofanous et al. [10,11]: "The commonality of the Kutateladze and Zuber ideas, expressing the external hydrodynamics control, boils down to scaling a critical vapor velocity in terms of the relevant fluid properties–densities and surface tension–and the body force field. There is no external length scale, and this implies a limitation to horizontal infinite flat plates. For both there is an ''internal'' length scale, the capillary length, and this provides an approximate measure of the dimensions above which the plate can be considered infinite… But there are also some basic differences in the two ways of thinking that have to be kept in mind in addressing issues of geometry, satisfying respectively self-similarity.

Zuber's postulated Rayleigh–Taylor controlled counter-current flow is macroscopic, and it is easy to see that self-similarity for it requires strict absence of external length scales able to introduce departures from (on the average) one-dimensional (1D) behavior [4]. In turn, this requires that the

liquid pool contains no bypass regions (its cross-section is fully coincident with the heater's cross-section), and that it is of small aspect ratio (height divided by the smallest lateral dimension)".

He further explains that Gaertner experiment [12] with a disk of the 5-cm diameter, placed on the bottom of a deep (20 cm) and wide (14 cm) reservoir with liquid, does not satisfy these requirements.

"Kutateladze's idea of ''repulsion'' is more vaguely stated, and thus it allows a somewhat greater flexibility in satisfying self-similarity. It appears that he is focused in a boundary layer, right next to the heater surface, and he thinks of a hydrodynamic transition occurring within this layer. Following his experiments with Gogonin [13], they assert that a width of even 2 capillary lengths (~2 mm in their ethanol experiments) is sufficient to eliminate the effect of an external length scale. Their water pool was deep (~15 cm) and much wider than their heater (10 cm). These experiments yielded the Ku = 0.145 result (as in Eq. (1)). Excellent agreement with Eq. (1) was also reported by Kutateladze and Malenkov in later water boiling experiments [14]. Unfortunately, no mention of the flow regimes observed was made in these papers, but Kutateladze had no doubt that the twophase flow above the heater was dispersed and highly chaotic (i.e., he disagreed with Zuber's picture of a relatively regular array of vapor jets). What remains unclear is the extent of interplay between the external hydrodynamics and the transition within the boundary layer that was the focus of Kutateladze's interest. In this interpretation both Gaertner's and Kutateladze's own experiments are open to question of such ''external'' influences. Remarkably, all other previous experiments are even further removed from these self-similarity requirements."

Theofanous et al. [11] propose to introduce the scale separation. They suppose that "Based on infrared thermometry, and aided by X-ray radiography data on void fraction, the case for a scale separation phenomenon in high heat flux pool boiling is argued. This indicates that boiling crisis is controlled by the microhydrodynamics and rupture of an extended liquid microlayer, sitting and vaporizing autonomously on the heater surface". They conclude: "Thus we can conclude that boiling heat transfer is independent of the complex two-phase flow hydrodynamics above the heater, and in particular that the previous hydrodynamic theory of boiling crisis is not appropriate". In the work of Yagov [15], a new model of liquid boiling crisis was developed based on the physical estimates of the process of evaporation of the thin liquid film menisci, adjacent to "dry spots" on the heating surface. The crisis beginning is associated with violation of the balance of liquid supplied to the "dry spot" boundary and evaporated liquid. The boiling crisis is explained as a result of coalescence and growth of the "dry spots" area on the heated surface. Calculation relations are obtained for the CHF at pool boiling in the region of low reduced pressures P_S/P_{cr} < 0.001 (P_S and P_{cr} are the saturation pressure and the critical pressure, respectively), for the region of high reduced pressures P_S/P_{cr} > 0.03, and the interpolation formula for CHF calculation at arbitrary pressure is derived. The calculated dependences are in good agreement with the experimental data. In most current experimental studies on heat transfer during boiling, the near-wall region, formation and growth of dry spots are investigated [10,11,16–18].

In [8], the authors specified the requirements for a setup to test the Zuber theory with a heater in the form of an infinite flat plate. For such a testing, to get rid of the horizontal inflow of liquid, which has a noticeable effect on CHF, it is necessary that the experimental conditions should be as close as possible to the theoretical model of the process on an infinite plate, i.e., the experimental heater should be a very clean plate with the dimensions much larger than λ_d limited by vertical lateral walls. It is shown in [20,21] that with the ratio of horizontal dimensions for a square plate $L/\lambda_d > 3$, where L is the side of a square plate, the surface can be considered an infinite plane.

In [22], Lienhard pointed out a number of erroneous assumptions, including the arbitrariness of some of relationships used in the Zuber model [3,4]. In [22], a number of unresolved issues in the hydrodynamic theory of boiling crises are presented. One of the questions concerns mainly the properties of the heating surface that are not taken into account by the Zuber theory. The second unresolved issue, considered in [22], is the question of where the Helmholtz instability occurs actually, on what scales from the heating surface. The problem with the Zuber crisis model is that in many cases it is difficult to identify the vapor jet behavior. As Lienhard writes in [22], Haramura and Katto

[23] suggested that the Helmholtz process does not develop in the obvious vapor jets and columns at all, but rather in a small structure of mini-jets near the surface that feed the visible jets from below. At its core, the theory of Haramura and Katto is also a substantiation of the hydrodynamic theory. However, in this theory, in contrast to the Zuber theory, a liquid film under a mushroom-shaped bubble, directly adjacent to the heating surface, is considered.

The works of Theofanous et al. [10,11] deny the influence of external (macro) hydrodynamics on the boiling crisis. They also question the influence of external hydrodynamics on the boiling crisis in the experiments of Gaertner [12] and Kutateladze [13,14]. At the same time, Theofanous remarks that, unfortunately, the observed flow regimes were not mentioned in Kutateladze works. In Gaertner experiments, large mushroom-shaped bubbles were observed in pre-crisis boiling regimes. The theory of Haramura and Katto was constructed on the basis of these observations [23]. It is believed that mushroom-shaped bubbles are formed by merging of several bubbles in a region of vapor (light phase) accumulation near the wall. The microhydrodynamics of the near-wall region affects the external (macro) hydrodynamics. To find out this influence, it is necessary to study the spatial distribution of such bubbles over the heating surface under the conditions of the infinite plane geometry proposed in [8], when the horizontal inflow of liquid is excluded.

As it was noted by Theofanous et al. [11], in the Zuber theory the ratio of the liquid layer height to the smallest transverse dimension must be small. The liquid layer must be of a finite height. Theofanous et al. [11] present experimental data on the crisis of water boiling at atmospheric pressure in a parallelepiped volume with height $H = 70$ mm and the smallest linear horizontal dimension $l = 35$ mm, i.e. $H / l = 2$, while the average void fraction $\varepsilon = 40\%$, (where ε is the ratio of the vapor volume to the entire volume of the system). Hence it follows that the height of the initial liquid layer at a temperature of 100°C is 42 mm. The wavelength of the Helmholtz instability plotted from the most dangerous wavelength of the Taylor instability is $\lambda_{Hd} = 2\pi(\lambda_d / 4) = 42.8$ mm. Perhaps, by pure chance, a layer of water with a height almost equal to the wavelength of the Helmholtz instability in the Zuber theory was used in the experiments of [11]. It is difficult to establish the upper limit of the layer height, when hydrodynamic boiling crisis is observed (the liquid is "pushed" from the heating surface by a vapor film). At the same time, there are thinner liquid films, when the boiling liquid film breaks down and the surface drying crisis is observed. In the geometry of an infinite plane [8], it is possible to establish the minimum height of the liquid layer, above which the usual hydrodynamic boiling crisis is observed, and in the thinner layers, the surface drying crisis is observed.

In the geometry of an infinite plane [8], when the heating surface is limited by vertical walls, the height of the two-phase layer of boiling liquid increases with an increase in its vapor content. One of the shortcomings of the Zuber theory is that, according to the theory, the vapor content of a liquid layer is $\pi/16$, while in experiments it is much higher. In the work of Kutateladze and Malenkov [14] on establishing the analogy between the process of nucleate boiling and bubbling, the influence of this parameter is also directly indicated.

In their previous work [24], the spatial distribution of mushroom-shaped bubbles over the heating surface is studied under the conditions of geometry of an infinite flat plate on a smooth heating surface. The effect of liquid layer height (n-dodecane) and void fraction on CHF and its mechanism is studied. Using the mathematical apparatus of the Zuber theory, the authors of this paper proposed a hydromechanical model of the nucleate boiling crisis, which takes into account the effect of void fraction on CHF. The theory of CHF is considered from the point of developed nucleate boiling using the mathematical apparatus of the Zuber theory.

In this paper, we present new experimental data on CHF during n-dodecane boiling on the surface of two 2D modulated capillary-porous coatings of the same morphology and geometry, made of different materials. Experiments are compared with theoretical calculations. New data on CHF for Novec – 7100 dielectric liquid on a smooth surface are also presented. A symmetric problem is considered: the Zuber problem in the traditional formulation with the involvement of new experimental data on observation of vapor columns in a liquid layer from the point of transitional boiling, in which the shortcomings of the known theory are eliminated. The numerical values of obtained solutions of one problem are compared, but with a symmetrical approach (in terms of

nucleate boiling and in terms of transitional boiling). Attention is paid to the analysis of the arrangement symmetry of the observed structures and the results of solving the problems.

2. Materials and Methods

The studies were carried out on an experimental setup consisting of a working chamber, a cooling system, a pressure and temperature measurement system, a system for collecting and processing test data, and a system for controlling the heaters power and supply. In **Figure 3 (a)**, the working chamber was mounted on a frame; the pressure in the working chamber was measured by two pressure sensors. The temperature was measured with thermocouples; the reduced pressure was created by a vacuum pump. The water flow in the cooling system of the working chamber was regulated by a rotameter; the temperature in the coil for heating the working chamber was kept constant by means of a thermostat while pumping the liquid. The ionization-deformation pressure sensor Setra-730 is used in the pressure range from 33 to 1333 Pa. The measurement error of this sensor is ± 0.5% of the current reading. The measurement range of the deformation - membrane pressure sensor ASG Edwards is from 133 to $2 \cdot 10^5$ Pa. The measurement error is ± 0.2% of the total scale. This sensor was used to measure pressures above 1000 Pa. Before each series of measurements, the sensor was calibrated based on the readings of a more accurate sensor (Setra-730) at low pressure, and then appropriate corrections were added to the measured data. The signals of pressure and temperature sensors were recorded using the National Instruments equipment and processed in the LabVIEW application environment. A detailed description of the setup is given in [25].
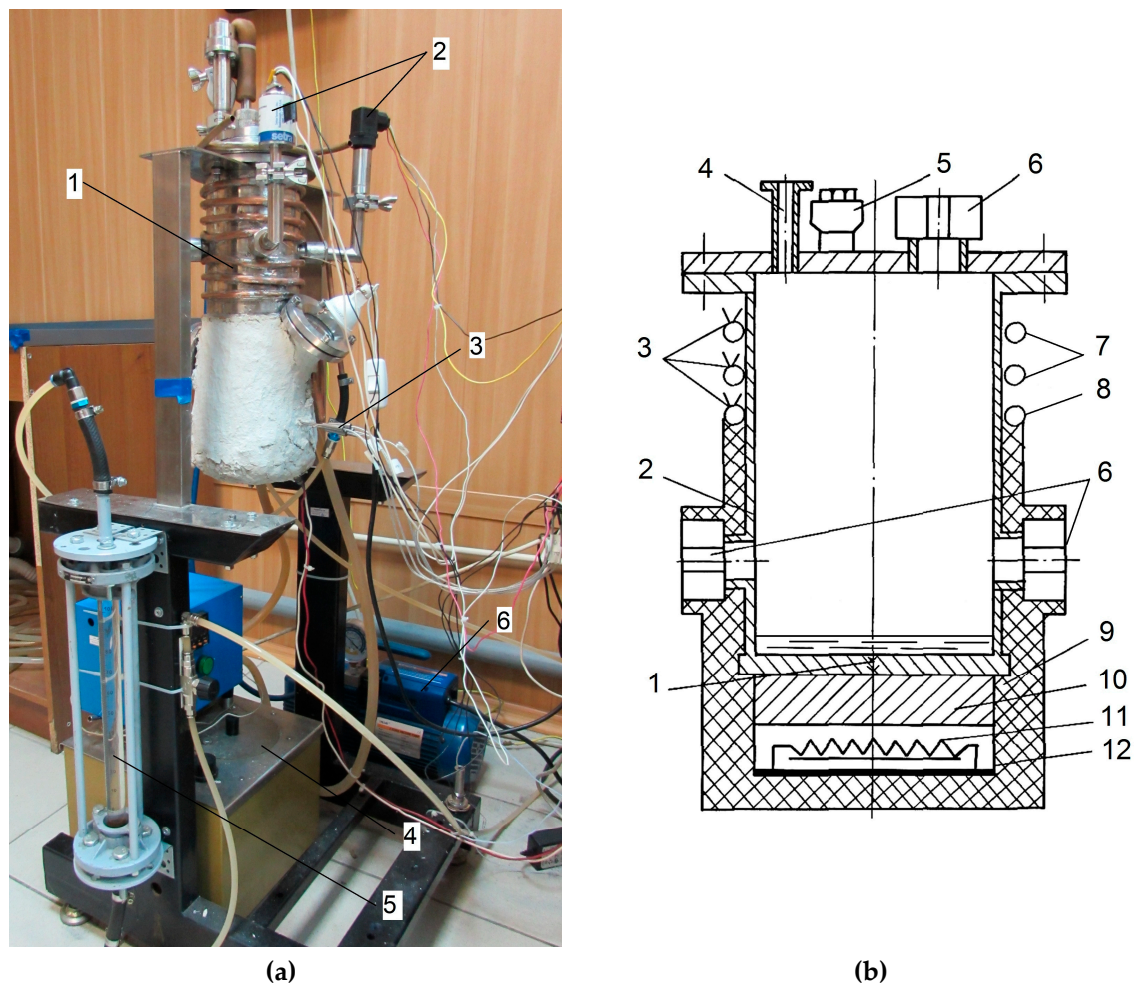

(a)   (b)

Figure 3. Experimental facilities: (a) –photograph of experimental setup: 1 –process chamber of experimental setup, 2 – pressure sensors, 3 – thermocouples for measuring the temperature of the heated surface, 4 – thermostat, 5 – rotameter, 6 – vacuum pump; (b) –process chamber of

experimental setup: 1 – bottom (smooth or with capillary-porous coating), 2 – case, 3 – thermocouples, 4 – branch pipe for fixing the pumping system, 5 – vacuum inlet, 6 – inspection windows, 7 – cooling coil, 8 – heating coil, 9 – thermal insulation layer, 10 – brass plate, 11 – electric heater, 12 – electric heater cover.

The working chamber was made in the form of a thermosyphon (**Figure 3 (b)**). It is a cylindrical vessel made of steel 12Kh18N10T with an inner diameter of 120 mm, a height of 300 mm, and a wall thickness of 1 mm. To achieve uniform distribution of the heat flux over the heated surface, a highly thermally conductive brass plate 30 mm thick was placed between the chamber bottom and a heater with a power of 2 kW. To reduce the contact thermal resistance, the gap between the chamber bottom and the plate was filled with a special highly thermally conductive paste. There is a cooling coil on the outer surface of the upper part of the chamber. The chamber is cooled by water flowing through a coil. To reduce heat loss due to leakage along the chamber walls from the bottom to the cooling coil and to ensure uniform temperature distribution at the chamber bottom, an additional coil for heating the chamber walls was mounted below the cooling coil. There were three inspection windows on the working chamber top and on its wall to perform visual observations. Two windows were used for observation and one window was used for illumination. The results of visual observations were recorded by a video camera with a shooting frequency of 24 fps and 240 fps. To measure the heating surface temperature, the copper-constantan thermocouples in stainless capillaries were inserted into five holes of 1.5-mm diameter in the bottom at different heights. The heat flux was determined from the temperature gradient measured along the bottom centerline using a linear Fourier approximation of the output signal of five thermocouples. The calculated error in determining the heat flux was about ± 16% for a heat flux $q = 10^3$ W/m², about ± 10% for a heat flux $q = 10^4$ W/m², and ± 4% for a heat flux $q = 10^5$ W/m². The surface temperature was determined by linear extrapolation of the measured temperature profile to the surface. The total error in measuring the surface temperature was no more than ± 0.4°C at 200°C. The pressure in the working chamber was kept constant. The lower horizontal surface (bottom) of the working chamber 12 mm thick, which is a horizontal smooth surface 120 mm in diameter with roughness Rz = 3.2 μm, bounded by the vertical walls of the chamber, was used as the heating surface. Two surfaces with capillary-porous coatings were also used. Coatings were applied to the working chamber bottom using SLM/SLS (Selective Laser Melting/Selective Laser Sintering) 3D laser printing technology.

N-dodecane was used as the working fluid. The physical properties of n-dodecane were calculated according to [26]. The experiments were carried out at pressure P_S (P_S / P_{cr}): 5 kPa ($2.8 \cdot 10^{-3}$), 10 kPa ($5.5 \cdot 10^{-3}$), and 20 kPa ($1.1 \cdot 10^{-2}$). When the pressure changed from 10 kPa to 20 kPa, the saturation temperature changed from 138.4°C to 158.3°C. The value of the capillary constant for n-dodecane varied from 1.53 mm to 1.46 mm; accordingly, the most dangerous length of the Taylor instability λ_d varied from 16.6 to 15.9 mm. There was the ratio L / λ_d ~ 7.2, that is, in terms of configuration and size, the heating surface is an infinite flat plate under the conditions of [8]. In this work, the layers of n-dodecane with a height of 1.7, 2.5, 4, and 10 mm were used. Some experiments on a smooth surface were carried out using the layer of Novec – 7100 dielectric liquid 10 mm high at a pressure of 100 kPa. The physical properties of Novec – 7100 were calculated according to [27,28]. The capillary constant of Novec – 7100 dielectric liquid at these pressures varies from 0.9 mm to 0.85 mm; therefore, the conditions of infinite flat plate geometry [8] can also be satisfied for this liquid.

2.1. Capillary-porous coatings

Capillary-porous coatings of stainless steel LPW 155 (15-5PH) and bronze powder AISI C836000 were applied to the lower base (bottom) of geometrically similar chambers specially made for each coating using laser 3D printing technology by the SLM/SLS method (selective laser melting / selective laser sintering). When applying coatings, special attention was paid to creating coatings of the same profile, with the same porosity and particle size, which remain in the porous structure. The coating technology is described in detail in [29,30].

The morphology of the stainless steel sample was analyzed using a Hitachi S-3400N scanning electron microscope, and the morphology of the bronze samples was analyzed using a Hitachi TM1000 microscope. A BRUKER Contour GT-K1 optical microscope profilometer was used to plot coating profilograms. Topographic maps with thickness distribution and SEM-images of the developed capillary-porous coatings No. 1, 2 are presented in **Figure 4**. According to the data obtained with the help of an optical microscope profilometer, the following characteristics of the coatings were determined: the height of ridges, the thickness of the residual layer between the ridges, and modulation wavelength λ_m. Porosity measurements were carried out by measuring the density of samples of 10 × 10 × 5 mm and comparing the results with the density of the coating material.
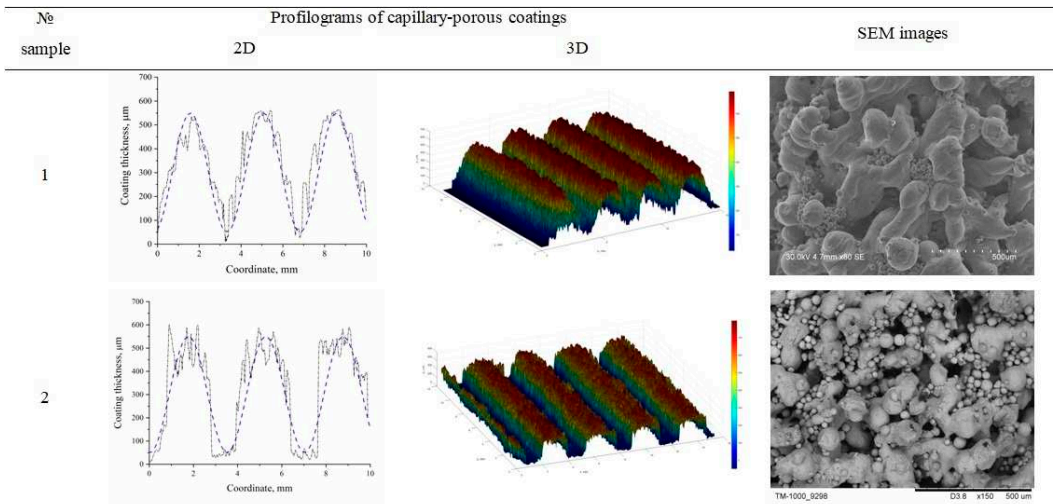

Figure 4. Profilograms and SEM images of capillary-porous coatings.

The parameters of capillary-porous coatings are presented in Table 1. The effective thermal conductivity of the coating was calculated using the formula:

$$k_{eff} = (2 - 3\ \phi)\ \lambda/2, \tag{3}$$

where ϕ is the coating porosity; λ is the thermal conductivity of the coating material. In [31], formula (3) was derived for the cases, when the thermal conductivity is much smaller than the thermal conductivity of the coating material.

Table 1. Parameters of capillary-porous coatings.

Parameter	Sample 1	Sample 2
Coating powder material	Stainless steel LPW 155 (15-5PH)	Bronze AISI C836000
Thermal conductivity of coating material	$\lambda \approx 20$ W/(m·K)	$\lambda \approx 89$ W/(m·K)
Porosity	$\phi = 44$ %	$\phi = 44$ %
Maximum height	$\delta = 550$ μm	$\delta = 550$ μm
Minimum height (residual layer)	$\delta_0 = 50$ μm	$\delta_0 = 50$ μm
Profile equation	$z = (A/2)\cdot\sin(2\pi x/\lambda_m) + A/2 + \delta_0$	
Amplitude	$A = \delta - \delta_0 = 500$ μm	$A = \delta - \delta_0 = 500$ μm
Modulation wavelength	$\lambda_{m1} = 3500$ μm	$\lambda_{m2} = 3500$ μm
Effective thermal conductivity of the coating k_{eff}*	$k_{St} = 6.8$ W/(m·K)	$k_{Br} = 30.6$ W/(m·K)

Thermal resistance at maximum coating height (ridge)	$\delta/k_{St} = 8.09\cdot10^{-5}$ (m$^2\cdot$K)/W	$\delta/k_{Br} = 1.8\cdot10^{-5}$ (m$^2\cdot$K)/W

3. Results

3.1. Results of visual observations and CHF measurements

In the regimes of developed nucleate boiling, the two-phase layer was represented by foam with "vapor columns" at the corners of a square array; one vapor column rose in the center (**Figure 5 (a)**). The vapor columns are symmetrical with respect to the square array center when rotating by an angle multiple of $\pi/2$, with respect to the axes passing through the square array diagonals, and also with respect to the axes passing through the center parallel to the sides of the square array. "Vapor columns" form, when large mushroom-shaped bubbles collapse. Theoretical models of instability [6,7,19] consider the instability at the gas-liquid interface. Both gas and liquid are considered as a continuous medium. In this case, it was found that the arrangement of large mushroom-shaped bubbles, formed as a result of merging of several small bubbles, obeys a certain pattern in a boiling liquid layer on the heating surface. The authors of this work were the first who recorded a two-dimensional instability of a boiling liquid layer by direct visual observations.
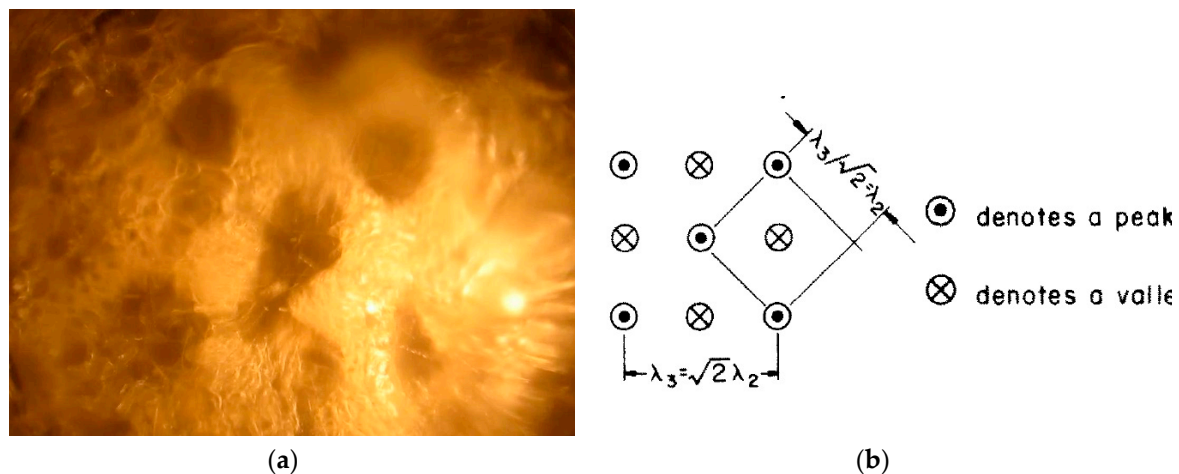

(a)   (b)

Figure 5. Two-dimensional instability of a boiling liquid layer: (a) – photograph of "vapor columns" in a thin n-dodecane layer at nucleate boiling: layer height h = 2.5 mm, volume pressure P_s = 20 kPa, q = 108 kW / m^2, temperature difference (T_w - T_s) = 42.1 K; (b) – top view of the liquid-vapor interface with two-dimensional Taylor instability [19].

The Taylor instability [6] was analyzed for two liquids, when the density of one liquid is greater than the density of the other and the gravity vector is directed towards the liquid with a lower density. In pre-crisis regimes and at the moment of crisis, the layer of boiling liquid is foam in its structure. The density of foam is greater than the density of a vapor phase. In this case, the main characteristic of foam is void fraction ε. Near the heating surface, at distances of 0.3–0.5 mm from the wall, the void fraction is ε = 0.85–0.92 and decreases with a height, see, for example, [11,32]. In [11,32], water was used as a working fluid. In [11] the study was carried out in a vessel with side walls, where the influence of a horizontal liquid inflow was excluded, but the dimensions of the heating surface were much smaller than those required according to [20,21] to consider the heating surface as an infinite plane. In [32], the heating surface was 29 mm in diameter, and a horizontal inflow of liquid was not ruled out. In both studies (as well as in many others) it is convincingly shown that the void fraction in the near-wall layer is much higher, therefore, the density of the two-phase system (foam) in this area is lower, therefore, conditions for origination of the Taylor instability are created.

The Taylor instability at the liquid-vapor interface for the two-dimensional case was analyzed by Sernas et al [19]. In 1969, the authors of [19] showed that two-dimensional wavelength of

instability λ_3 is larger than one-dimensional wavelength λ_2 by a factor of $\sqrt{2}$ (see **Figure 5 (b)**). In addition, according to the analysis [19], in the two-dimensional case of Taylor instability, there should be one more peak at the center of the array. The peaks in **Figure 5 (b)** correspond to "vapor columns". Zuber in his analysis used the length of the critical instability wave λ_{cr} and the length of the most dangerous wave λ_d, obtained in [7] for the one-dimensional case of Taylor instability. The proposed Zuber geometry takes the form of a square area with side λ_2, as it is shown in **Figure 5 (b)**. As it follows from comparison of the photograph and the scheme shown in **Figure 5**, in this case it was possible to fix an image of the two-dimensional instability of the boiling liquid layer on a horizontal surface.

To obtain quantitative characteristics of the observed phenomenon, the diameter of vapor columns d_v and the distance between their centers l_v were measured from video frames. Table 2 shows the experimental results for the layers of n-dodecane on a smooth surface and on capillary-porous coatings, as well as for a layer of Novec - 7100 liquid, boiling on a smooth surface.

Table 2. Linear dimensions.

Regime		l_σ, mm	λ_{cr}, mm	λ_d, mm	h, mm	d_v, mm	l_v, mm	(d_v/l_v)
P, kPa	T_s, °C							
N-dodecane, smooth surface								
10	138.4	1.53	9.59	16.6	2.5	13.4	31	0.43
					4.0	14.7	32	0.46
20	158.3	1.46	9.18	15.9	2.5	12.5	32	0.39
					4.0	11.7	31	0.38
N-dodecane, 2D modulated stainless steel capillary-porous coating								
5	120.7	1.58	9.93	17.2	4.0	12.9±0.1	24.2±0.2	0.53
10	138.4	1.53	9.59	16.6	4.0	14.6±0.2	24.3±0.2	0.6
N-dodecane, 2D modulated bronze capillary-porous coating								
5	120.7	1.58	9.93	17.2	4.0	12.6±0.1	24.1±0.1	0.52
10	138.4	1.53	9.59	16.6	4.0	12.4±0.2	25.6±0.1	0.48
Dielectric liquid Novec-7100, smooth surface								
100	61	0.85	5.33	9.23	10.0	–	20.3	–

The values of capillary constant, the critical and the most dangerous wavelengths of Taylor instability are also presented in Table 2. The error in measuring the diameter of vapor columns d_v and the distance between their centers l_v during boiling on a smooth surface is estimated as ±12%. The errors in measuring the diameters of vapor columns and the distances between them on the surface with a capillary-porous coating are given in Table 2. It can be seen from the Table that the distance between the centers of vapor columns during boiling on a smooth surface is slightly less than the doubled length of the most dangerous Taylor instability wave. The ratio of vapor column diameters to the distance between their centers during boiling on a smooth surface is somewhat less than 0.5, while in the Zuber theory [3,4] this ratio is taken equal to 0.5. In the Novec - 7100 dielectric liquid layer, the vapor column diameter could not be measured. The distance between large bubbles, formed at the site of vapor column destruction under the liquid layer was measured at the upper boundary of the liquid layer. The distance between the centers of vapor columns on surfaces with capillary-porous coatings was less than that on a smooth surface, while the diameters of vapor columns were approximately the same in both cases.

The results of the CHF measurement are shown in **Figure 6**. Unfilled symbols indicate data obtained on a smooth surface. For a layer with an initial height of 4 mm, experimental data on CHF on surfaces with a capillary-porous coating are also presented. Half-filled symbols indicate experimental data obtained on a capillary-porous stainless steel coating (sample 1). Crossed symbols

denote experimental data obtained on a bronze capillary-porous coating (sample 2). For liquid layers with a height of 1.7 mm, in an n-dodecane layer on a smooth surface, a crisis of surface drying was observed. When the CHF was achieved in the middle of the heating surface, the liquid layer height decreased and a stable dry spot was formed. In the pre-crisis regime and during the crisis, a mass ejection of drops and bubbles from the liquid layer was observed. In layers of a greater height, both on smooth surfaces and on surfaces with a capillary-porous coating, a hydrodynamic crisis of nucleate boiling was observed. The liquid layer was pushed aside the heating surface, there was a vapor film under this layer, and the surface temperature increased rapidly. It can be seen from **Figure 6** that the CHF on a smooth surface in a 1.7-mm layer, corresponding to the crisis of surface drying is less than the CHF in layers of a larger height, where the hydromechanical crisis of nucleate boiling occurs. Experimental data scattering exceeds the errors of experimental measurements of the heat flux densities. It can be observed that in the layer with an initial height of 10 mm, the CHF is also less than in the layers of a smaller height. There is some certain height of a liquid layer, corresponding to the maximum CHF. The generalizing diagram of the effect of liquid layer height on CHF is shown in [25]. The lines corresponding to the known dependences [1–4,9,15] for calculating the CHF during pool boiling on smooth surfaces are presented in **Figure 6**. Experimental data deviate from calculation dependences significantly. According to **Figure 6**, the CHF on the surface with a capillary-porous coating exceeds the maximum CHF on a smooth heating surface by more than 1.5 times.
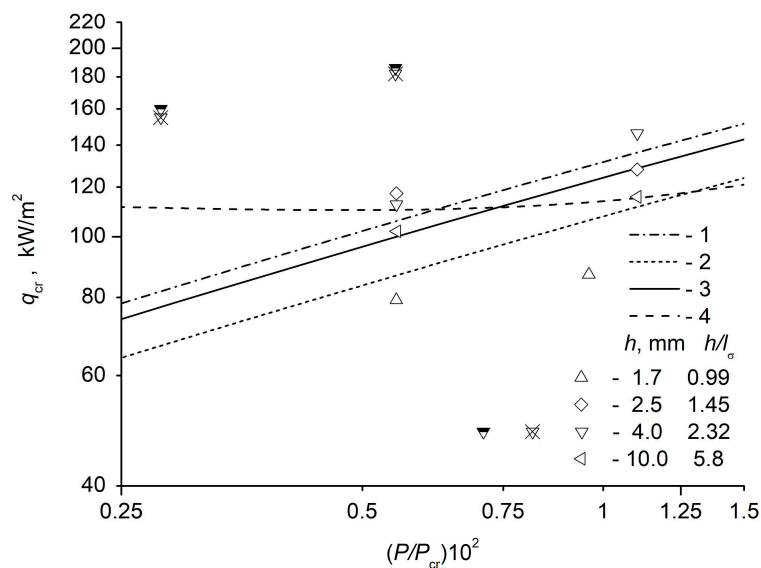

Figure 6. The critical density of the heat flux. Calculated dependences: 1 – calculation by Kutateladze formula (1); 2 – calculation by Zuber equation (2); 3 – calculation by dependence [9]; 4 – calculation by Yagov equation [15].

3.2. Hydrodynamic model of CHF. Developed nucleate boiling approach

In calculations, foam above the near-wall region around vapor columns was considered as an isotropic homogeneous system with void fraction ε, some average temperature T_f, pressure P_f and density ρ_f. This is a common approach to solving such problems [33]. A detailed derivation of equations is given in [24]. For the most dangerous wavelength of the considered instability in the foam layer, in [24] it was obtained:

$$\lambda_{fd} = 2\pi(3\sigma / g(\rho_f - \rho_v))^{1/2} \tag{4}$$

The density of foam is expressed in terms of void fraction as follows:

$$\rho_f = \varepsilon\rho_v + (1-\varepsilon)\rho_l .$$

Let us express the density difference in the denominator of (4) in terms of void fraction and liquid density:

$$\rho_f - \rho_v = (1-\varepsilon)(\rho_l - \rho_v). \tag{5}$$

Substituting the relation (5) into (4), we obtain that the length of the most dangerous Taylor instability wave at the vapor-foam interface is expressed in terms of the instability wavelength at the liquid-vapor interface:

$$\lambda_{fd} = (1-\varepsilon)^{-1/2} \lambda_d. \tag{6}$$

The void fraction was determined from the distance between vapor column centers measured in experiments. The values $l_v = \lambda_{fd}$ were equated and an expression for void fraction calculation was obtained from relation (6):

$$\varepsilon = 1 - \left[\frac{2\pi\sqrt{3}l_\sigma}{l_v}\right]^2 \quad \varepsilon = 1 - \left(\frac{2\pi l_\sigma \sqrt{3}}{l_v}\right)^2.$$

The calculated values of void fraction obtained are given in Table 3. The calculated CHF values are compared with the experimental values in the same Table 3.

Table 3. Comparison of CHF calculation with experiments.

Regime		h, mm	ε	q_{cr}, kW/m² experiment	q_{crt}, kW/m² calculation	$\frac{\|q_{cr} - q_{crt}\| \cdot 100\%}{q_{cr}}$
P, kPa	T_s, °C					
N-dodecane, smooth surface						
		2.5	0.713	117.3	118.5	1
10	138.4	4.0	0.731	112.6	111.2	1.2
		10.0	0.75	102	103	1
		2.5	0.745	128	131	2.3
20	158.3	4.0	0.737	146	140	4.1
		10.0	0.78	115.8	117	1
N-dodecane, 2D modulated stainless steel capillary-porous coating						
5	120.7	4.0	0.494	165	160	4.2
10	138.4	4.0	0.533	186	193	3.5
N-dodecane, 2D modulated bronze capillary-porous coating						
5	120.7	4.0	0.49	155	161	4.0
10	138.4	4.0	0.579	182	174	4.7
Dielectric liquid Novec-7100, smooth surface						
100	61	10	0.793	151.6	148	2.5

To calculate CHF, we used the formal mathematical apparatus developed by Zuber [3,4]. Formulas for calculating CHF are derived in [24]. Here, only the main relations are presented with some explanations, not reflected in [24]. To calculate CHF, the following expression was obtained in [24]:

$$q_{crt} = h_{LG} \rho_v \left(\frac{A_v}{A}\right) \left(\frac{\sigma m}{\rho_v}\right)^{1/2} \left(1 + \frac{\rho_v}{\rho_f}\right)^{1/2}, \tag{7}$$

where (A_v / A) is the ratio of the area of the vapor column cross-section to the area of the surface from which it rises.

In [34], the critical heat fluxes and separation diameters of bubbles were studied at heat fluxes close to and equal to CHF on a flat heating surface in the pressure range from 0.1 to 7 MPa. The paper shows that the maximum diameter of coalesced bubbles is close to the Taylor instability wavelength in the studied pressure range. In [24], it is considered that vapor columns are formed as a result of transformation of these large hemispherical coalesced bubbles, whose diameter at the moment of

transformation beginning is equal to the length of the most dangerous Taylor instability wave, derived from the liquid density. This means that the dimensions of vapor columns do not depend on the void fraction of the liquid layer, while the distance between the centers of bubbles depends on ε; therefore, depending on the void fraction, the area ratio (A_v / A) will change. Further, this bubble transforms into a vapor column in the form of a cylinder with the same volume as the bubble and a height equal to the bubble height ($0.5\lambda_d$)

Equating the wavelength of Helmholtz instability to the vapor column radius, we obtain:

$$\lambda_{Hf} = (1/6)^{1/2}\lambda_d$$

The CHF density after substituting all values into (7) is equal to:

$$q_{crt} = \frac{\pi}{6}(1-\varepsilon)2^{1/4}h_{LG}\rho_v\left(\frac{\sigma g(\rho_l - \rho_v)}{\rho_v^2}\right)^{1/4}\left(1+\frac{\rho_v}{\rho_f}\right)^{1/2}, \qquad (8)$$

where value

$$k = \frac{\pi}{6}(1-\varepsilon)2^{1/4} = 0.623(1-\varepsilon) \qquad (9)$$

is usually called the Kutateladze constant.

As it follows from Table 3, the maximum deviation of calculated CHF values from those obtained in experiments is 4.7%. It also follows from Table 3 that the void fraction in the layer on capillary-porous surfaces is less than that on a smooth surface, and the CHF value is greater. A decrease in the void fraction in the layer on capillary-porous surfaces may relate to a decrease in the separation diameters of bubbles on these surfaces as compared to the smooth ones. A decrease in separation diameters of bubbles during liquid boiling on porous surfaces relative to the data obtained on smooth samples is noted in many papers, for example [35–38]. According to the data of [39], bubble rise according to the Stokes law, when the rate of bubble rise increases with increasing diameter, is observed up to Reynolds numbers Re = 450. For n-dodecane, under the experimental conditions, these bubble sizes are $d_b \approx 0.19$ mm. The rise rate of bubbles with a larger diameter is described by dependence:

$$u_b = \left(\left(\frac{2.14\sigma}{\rho d_b}\right) + 0.505 g d_b\right)$$

Since the vapor density is much less than the density of liquid, it can be neglected and this expression can be written in the following form:

$$u_b = \left(\frac{2.14 l_\sigma^2}{d_b} + 0.505\, d_b\right)^{1/2}\sqrt{g} \qquad (10)$$

The function defined by formula (10) has a minimum at $d_b \approx 2.06 l_\sigma$, for n-dodecane it is approximately 3.25 mm. Therefore, in the range of separation diameters of n-dodecane bubbles from 0.19 mm to 3.25 mm, the rate of bubble rise will increase with a decrease in their separation diameters. Bubble diameters in the foam layer, measured from the photograph (see **Figure 5 (a)**) are approximately 2-3 mm. On a capillary-porous surface, the separation diameters of bubbles are smaller, their rise rate is higher, the vapor phase is carried away faster, and the vapor content is less than on a smooth surface.

A two-phase system is called foam if the void fraction of this system is $\varepsilon \gtrsim 0.5$. In this case, the process on surfaces with coatings occurs in a foam layer with a limiting value of void fraction. Perhaps, this is some limiting case that can be described using this model. The boiling process on capillary-porous coatings is much more complicated, and the influence of not all parameters can be taken into account in this model. The given example shows that the processes in the near-wall region (microhydrodynamics) affect the external hydrodynamics.

An idea about the physics of crisis phenomena development is expressed in [18]. Within the framework of the model [18], it is assumed that the crisis is achieved due to the development of the Landau instability on the free surface of liquid films in the macrolayer under large vapor conglomerates. Therefore, the CHF value is proportional to the area of the wetted surface S_{wet} in the pre-crisis regime. In this case, $k \sim (1 - \varepsilon) \sim S_{wet}$, since the area of the wetted surface decreases usually

with increasing vapor content. The result obtained does not contradict modern ideas about the physics of crisis phenomena development.

For values of constant *k* varying within 0.13–0.19, as recommended by Kutateladze in [1,2], the corresponding calculated void fraction ε varies within 0.791–0.694. The values of void fraction coincide actually with the range of its change obtained in the work of Kutateladze and Malenkov [40]. In bubbling processes, the void fraction is proportional to the reduced gas velocity *u* ~ ε at constant pressure. The criterion for hydrodynamic stability of a two-phase layer during bubbling is expressed by the formula:

$$k = u_{cr} \left(\frac{\rho_v^2}{g\sigma(\rho_l - \rho_v)} \right)^{1/4},$$

that is, if we consider the bubbling process at constant pressure, then we get *k* ~ ε. Therefore, with small changes in the critical velocity u_{cr}, the *k* criterion will increase with increasing void fraction, while at CHF, according to relation (9) of this work, the Kutateladze constant will decrease.

The resulting expression (8) describes CHF through the parameters of external hydrodynamics. Until the very moment of the crisis, the liquid layer is in contact with the heating surface. Therefore, any process from six different CHF mechanisms, prevalent in the literature, can be a trigger of the boiling crisis: bubble interference [41], hydrodynamic instability [3,4], macrolayer dryout [23], hot/dry spot [11,15], interfacial lift-off [9,42], and model of multilayer liquid film adsorption under a vapor mass [43]. In this model, these mechanisms are not considered in detail. Processes directly on the heating surface change the structure of the near-wall layer with an increase in the heat flux, affect the external hydrodynamics through the vapor content, separation sizes of the bubbles, and changes in the instability wavelength, and, ultimately, affect the CHF value.

3.3. Symmetrical problem. Transitional boiling approach (Zuber problem)

In the Zuber theory of boiling crisis [3,4], a vapor film already formed on the heating surface is considered; the approach to boiling crisis is considered from the point of the transitional boiling regime. It does not take into account the conditions on the heating surface, and there is a problem with identification of "vapor columns".

As it was noted by Theofanous et al. [11], in the Zuber theory the ratio of the height to the smallest transverse dimension must be small. If we consider the boiling crisis model in the infinite plane approximation [8], then the liquid layer must also be of a finite height. In most experiments, the heater dimensions are usually identified, but the height of the liquid layer is not reported.

In [25], the authors of this paper give a photograph of the liquid layer (n-dodecane) obtained 5 seconds after the crisis (see **Figure 7**).
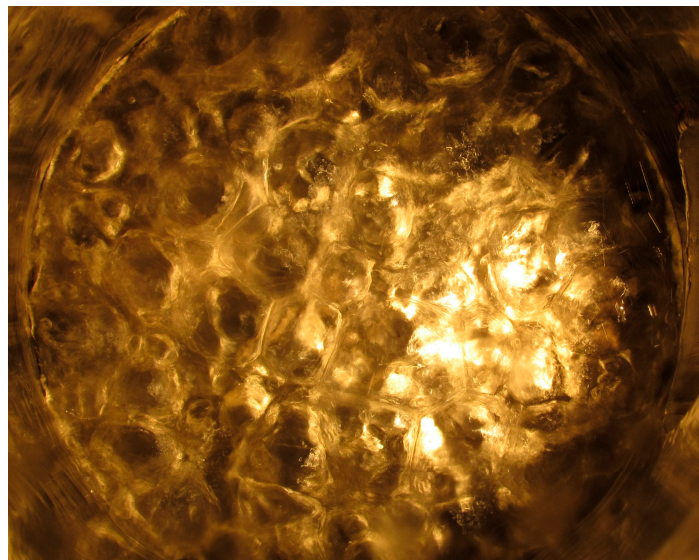
Figure 7. The layer of boiling liquid above the vapor film at the moment of crisis. Layer height h = 4 mm, at the moment of crisis: pressure P_s = 20 kPa (P_s/P_{cr} = 0.011), q = 146 kW/m², $T_w - T_s$ = 34.3 K. The Figure is taken from [25].

The liquid layer structure after the crisis changes dramatically. The layer of foam with vapor columns in pre-crisis regimes (**Figure 5 (a)**) passes into the layer of vapor columns with rising densely packed bubbles of almost the same size (**Figure 7**). The sizes of large bubbles are almost equal to the length of the most dangerous wave of the Taylor instability λ_d. Under conditions of a pool boiling crisis in the infinite plane approximation, when the layer is high, these vapor columns cannot be observed, apparently due to hydrodynamic instability, as it should be. In [25], during the study of boiling crises in n-dodecane layers on a smooth surface, such a pattern was observed only in layers 4 mm high. Below each bubble in the photograph, there is another column of bubbles that replace the top bubble when it collapses. Vapor rises up along the vapor columns and liquid moves down along the menisci at the bubble boundary. Taking a bubble collapse pattern in which at one moment bubbles burst simultaneously at the sites, corresponding to the peaks in **Figure 5 (b)** and at the next moment bubbles burst simultaneously at the sites of trough locations, we obtain the process flow diagram shown in **Figure 8 (a)**. Since the bubble diameters in **Figure 7** are equal to λ_d, then in **Figure 8 (a)** the wavelength for a two-dimensional instability will be equal to $\lambda_3 = 2\lambda_2 = 2\lambda_d$, where $\lambda_2 = \lambda_d$ is the most dangerous wavelength of the Taylor instability, obtained for the one-dimensional case in [7]. The side of the square grid corresponding to Zuber geometry will be equal to $\sqrt{2}\lambda_2 = \sqrt{2}\lambda_d$, as it is shown in **Figure 8 (a)**. The proposed Zuber scheme for the arrangement of vapor columns (**Figure 8**), depicted in the form of a figure by the authors of [21], takes the form corresponding to experimental observations (**Figure 8 (b)**).
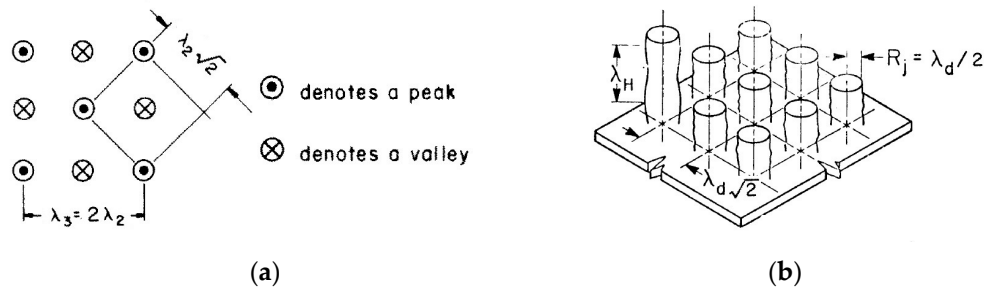

(a)   (b)

Figure 8. Calculation diagrams for CHF in terms of transition boiling approach. (a) top view of the liquid-vapor interface with a two-dimensional Taylor instability [19]; (b) layout of vapor columns on an infinite horizontal surface based on visual observations.

In the diagram (**Figure 8 (a)**) $\lambda_2 = \lambda_d$, so the side of the square grid is $\lambda_d\sqrt{2}$, the length of the most dangerous Taylor instability wave is $\lambda_d = 2\pi l_\sigma \sqrt{3}$, the vapor column radius is $R_j = \lambda_d / 2$, the Helmholtz instability wavelength is $\lambda_H = 2\pi R_j = \pi \lambda_d$, the velocity at which the vapor jets become unstable, according to Helmholtz, is $U_H = (\sigma m / \rho_v)^{1/2}$, and the wave vector is $m = 2\pi / \lambda_H$. Substituting these values into the general expression for the critical heat flux [21]:

$$q_{cr} = h_{LG}\rho_v \left(\frac{A_v}{A}\right) U_H ,$$

we obtain:

$$q_{cr} = 0.168 h_{LG}\rho_v \left(\frac{\sigma g(\rho_l - \rho_v)}{\rho_v^2}\right)^{1/4} . \tag{10}$$

16

For the considered regime of n-dodecane boiling on a smooth surface at a pressure of 20 kPa in a layer 4 mm high (see Table 3), the experimentally determined value of the critical heat flux is 146 kW/m². When calculating by formula (10), the heat flux is 143 kW/m²; the difference is 2%.

If vapor columns are located, as it is shown in **Figure 8 (a)**, the columns corresponding to the peaks work first, and then the columns corresponding to the troughs work; then in each cycle of "work", $(A_v / A) = \pi / 8$. **Figure 8 (b)** shows only the "working" columns. Due to the symmetry of arrangement of columns corresponding to peaks and troughs (see **Figure 8 (a)**), this scheme of the process does not change over time, regardless of the working column (corresponding to peaks or troughs). However, columns that do not "work" ", at a certain point in time, are also filled with vapor, so the ratio for the entire liquid layer is twice as large. Therefore, the void fraction of the layer in this model is equal to $\varepsilon = \pi / 4$, which is in good agreement with the experimental data.

When calculating the CHF using the first part of the model, implementing the nucleate boiling approach, the Kutateladze constant for the regime of n-dodecane boiling on a smooth surface at pressure of 20 kPa in a layer with an initial height of 4 mm (see Table 3) and void fraction ε = 0.737 is $k = 0.623(1-\varepsilon) = 0.623(1-0.737) = 0.164$. Comparison with formula (10) shows that the difference is ≈ 2.4%. At pressure of 10 kPa (see Table 3) in a layer with an initial height of 4 mm, the void fraction is ε = 0.731, k = 0.168, which coincides with the calculation by formula (10). Thus, for a smooth surface, numerical calculations show that the results of solution with different approaches are equivalent.

4. Discussion

This paper does not consider any mechanism triggering the boiling crisis. Regardless of the specific mechanism that determines the critical heat flux value during boiling, the crisis development is ultimately caused by the process of a sharp increase in the relative share of the area occupied by dry spots formed in a macrolayer near the heat-releasing surface. In the calculated dependence obtained using the mathematical apparatus proposed by Zuber, when the crisis is considered in terms of developed nucleate boiling, one more important parameter is introduced: void fraction of the boiling liquid layer under the conditions of infinite plane geometry. Obviously, the relative share of the area occupied by dry spots formed in a macrolayer near the heat-releasing surface depends on the void fraction of the liquid layer. The void fraction content cannot take into account the effect of all parameters; however, it can be measured in several independent ways, which allows identification of this parameter effect, especially when boiling on coatings. New experiments are required, when the layer void fraction would be measured, for example, using X-ray, capacitive methods, and adapted optical methods.

It is necessary to study the structure of a two-phase layer, the dependence of the wetted surface share, void fraction, and the size of bubbles in the foam layer on the heat flux at various reduced pressures and with varying the wetting properties of the heat-releasing surface, the thermal diffusivity, and the heater wall thickness.

Most of the results of research on the process of liquid boiling were obtained in experiments where water was used as a working fluid. For water boiling at atmospheric pressure, the length of the most dangerous Taylor instability wave is λ_d = 27.2 mm; then, to observe confidently the two-dimensional instability of the boiling water layer, as in this work, the characteristic diameter of the heating surface should be approximately equal to 7 λ_d ≈ 190 mm. Considering that the CHF for water boiling is much higher than that for n-dodecane, the creation of heating surfaces of such a diameter presents great technical difficulties and has not been implemented in any known scientific experiment on water boiling.

5. Conclusions

This model considers CHF in a horizontal liquid layer of a finite height, based on the visual observation of "vapor columns", both in terms of developed nucleate boiling and transitional boiling (a symmetrical problem).

In both cases, the solution of the problem is expressed through the same parameters of external hydrodynamics, the difference lies in the form of writing the Kutateladze constant. In the approach of developed nucleate boiling, the Kutateladze constant depends on the void fraction. Despite the difference in writing the Kutateladze constant, numerical calculations show the equivalence of the experimental results description.

In the first part of the solution (the developed nucleate boiling approach), the contact of liquid with the heating surface is taken into account; therefore, any of the currently known mechanisms can be the mechanism for the boiling crisis beginning.

As a result of processing experimental data for liquid layers, it was shown that the conditions on the heating surface (the presence of capillary-porous coatings) affect the void fraction of the layer, and thus their effect on CHF is taken into account.

References

1. Kutateladze, S.S. Hydromechanical model of heat transfer crisis in free-convection boiling. *Zh. Tech. Phys.* **1950**, *20*(11), 1389–1392.
2. Kutateladze, S. S. Hydrodynamic theory of boiling regime transition in free convection. *Izv. Akad. Nauk SSSR. Otd. Tekh. Nauk* **1951**, *4*, 529-536.
3. Zuber, N. Hydrodynamic Aspects of Boiling Heat Transfer (thesis), California. Univ., Los Angeles; and Ramo-Wooldridge Corp., Los Angeles, 1959.
4. Zuber, N. On the stability of boiling heat transfer. *Trans. ASME* **1958**, *80*, 711 – 720.
5. Westwater, J.W., Santangelo, J.G. Photographic Study of Boiling. *Ind. Engr. Chem.* **1955**, *47*, 1605-1610.
6. Taylor, G.I. The Instability of Liquid Surfaces When Accelerated in a Direction Perpendicular to Their Plane. *Proc. Roy. Soc. London, Series A* **1950**, *201*, 192–196.
7. Bellman, R., Pennington, R.H. Effects of surface tension and viscosity on Taylor instability. *Quart. Appl. Math.* **1954**, *12*, 151-162.
8. Lienhard, J. H., Dhir, V.K. Hydrodynamic prediction of peak pool-boiling heat fluxes from finite bodies. *Trans. ASME J. Heat Transfer* **1973,** *95* 152-158.
9. Mudawar, I., Howard, A. H., Gersey C.O. An analytical model for near-saturated pool boiling critical heat flux on vertical surfaces. *Int. J. Heat Mass Transfer* **1997**, *40*, 2327–2339.
10. Theofanous, T.G., Tu, J.P., Dinh, A.T., Dinh, T.N. The boiling crisis phenomenon: Part I: nucleation and nucleate boiling heat transfer. *Experimental Thermal and Fluid Science* **2002,** *26*, 775-792.
11. Theofanous, T.G., Tu, J.P., Dinh, A.T., Dinh, T.N. The boiling crisis phenomenon: Part II: dryout dynamics and burnout. *Experimental Thermal and Fluid Science* **2002**, *26*, 793-810.
12. Gaertner, R.F. Photographic Study of Nucleate Pool Boiling on a Horizontal Surface. *Trans. ASME, Ser C, J. Heat Transfer* **1965,** *87*(17), 17-29.
13. Gogonin, I.I., Kutateladze, S.S. Critical heat flux as a function of heater size for a liquid boiling in a large enclosure. *J. Eng. Phys.* **1977**, *33*, 1286–1289.
14. Kutateladze, S.S., Malenkov, I.G. Hydrodynamic analogy between heat transfer and nucleate boiling crisis in boiling and bubbling, Exp. data. *Heat Transfer–Soviet Res.* **1984**, *16*(4), 1–46.
15. Yagov, V.V. Is a crisis in pool boiling actually a hydrodynamic phenomenon? *Int J. Heat Mass Transfer* **2014**, *73*, 265–273.

16.   Surtaev, A.S., Serdyukov, V.S., Zhou, J., Pavlenko, A.N., Tumanov V. An experimental study of vapor bubbles dynamics at water and ethanol pool boiling at low and high heat fluxes. *Int. J. Heat Mass Transfer* **2018**, *126*, 297–311.

17.   Kim, H., Kim, D.E. Effects of surface wettability on pool boiling process: Dynamic and thermal behaviors of dry spots and relevant critical heat flux triggering mechanism. *Int. J. Heat Mass Transfer* **2021**, *180*, 121762.

18.   Pavlenko, A.N. "On the physics of the development of boiling crisis phenomena (comments on the article of E. D. Fedorovich "On the expediency of developing a two-stage model of boiling crisis of a liquid wetting a heating surface")," *Therm. Eng.* **2020**, *67*, 853–859.

19.   Sernas, V., Lienhard, J.H., Dhir, V.K. The Taylor wave configuration during boiling from a flat plate. *Int. J. Heat Mass Transfer* **1973**, *16*, 1820-1821.

20.   Lienhard, J.H., Dhir, V.K., Riherd D.M. Peak Pool Boiling Heat-Flux Measurements on Finite Horizontal Flat Plates. *Trans. ASME J. Heat Transfer* **1973**, *95*, 477–482.

21.   Lienhard, J.H., Dhir, V.K. Extended Hydrodynamic Theory of the Peak and Minimum Pool Boiling Heat Fluxes, NASA Report No. CR-2270, University of Kentucky, Lexington, 1973.

22.   Lienhard, J.H. Snares of pool boiling research: putting our history to use, in: Proceedings of the 10th International Heat Transfer Conference, vol. 1, Brighton, UK, 1994, pp. 333–348.

23.   Haramura, Y., Katto, Y. A new hydrodynamic model of critical heat flux, applicable widely to both pool and forced convection boiling on submerged bodies in saturated liquids. *Int. J. Heat Mass Transfer* **1983**, *26*, 389-399.

24.   Zhukov, V.I., Pavlenko, A.N. Crisis of nucleate boiling in a finite-height horizontal layer of liquid. *J. Engin. Thermophys.* **2020**, *29*, 1–13.

25.   Zhukov, V.I., Pavlenko, A. N. Heat transfer and critical phenomena during evaporation and boiling in a thin horizontal liquid layer at low pressures. *Int. J. Heat Mass Transfer* **2018**, *117*, 978–990.

26.   Yaws, C. L. *Handbook of Thermodynamic and Physical Properties of Chemical Compounds*, Knovel: NY, 2003, P. 597.

27.   3M™ Novec™ Engineered Fluid HFE-7100 Physical Properties.

28.   Rausch, M.H., Kretschmer, L., Will, S., Leipertz, A., Fröba, A.P. Density, Surface Tension, and Kinematic Viscosity of Hydrofluoroethers HFE-7000, HFE-7100, HFE-7200, HFE-7300, and HFE-7500. *J. Chem. Eng. Data* **2015**, *60*, 3759–3765.

29.   Bessmeltsev, V.P., Pavlenko, A.N., Zhukov, V.I. Development of a technology for creating structured capillary-porous coatings by means of 3D printing for intensification of heat transfer during boiling. *Optoelectronics, Instrumentation and Data Processing* **2019**, *55*, 554–563.

30.   Zhukov, V.I., Pavlenko, A.N., Shvetsov, D.A. The effect of pressure on heat transfer at evaporation/boiling in horizontal liquid layers of various heights on a microstructured surface produced by 3D laser printing. *Int. J. Heat and Mass Transfer* **2020**, *163*, 120488.

31.   Bodla, K.K., Murthy, J.Y., Garimella, S.V. Direct simulation of thermal transport through sintered wick microstructures, *J. Heat Transfer* **2012**, *134*, 012602.

32.   Iida, Y., Kobayasi, K., Distributions of Void Fraction above a Horizontal Heating Surface in Pool Boiling. *Bull. JSME*, **1969**, *12*, 283–290.

33.   Nakoryakov, V.E.; Pokusaev, B.G.; Shreiber, I.R. Wave Propagation in Gas-Liquid Media, *CRC Press* **1993**, 222 pp.

34.   Sakashita, H., Ono, A. Boiling behaviors and critical heat flux on a horizontal plate in saturated pool boiling of water at high pressures. *Int. J. Heat Mass Transfer* **2009**, *52*, 744–750.

35.   Cao, Z., Wu, Z., Sunden, B. Heat Transfer Prediction and Critical Heat Flux Mechanism for Pool Boiling of NOVEC-649 on Microporous Copper Surfaces. *Int. J. Heat Mass Transfer* **2019**, *141*, 818–834.

36.   Tang, K., Bai, J., Chen, S., Zhang, S., Li, J., Sun, Y., Chen, G. Pool Boiling Performance of Multilayer Micromeshes for Commercial High-Power Cooling. *Micromachines* **2021**, *12*, 980.

37.   Pavlenko, A.N., Kuznetsov, D.V., Bessmeltsev, V.P. Heat Transfer Enhancement during Pool Boiling of Nitrogen on Porous Coatings Produced by Selective Laser Melting/Sintering (SLM/SLS). *J. Engin. Thermophys.* **2022**, *31*, 1–10.

38.   Kuznetsov, D.V., Pavlenko, A.N. Heat Transfer during Nitrogen Boiling on Surfaces Modified by Microarc Oxidation. *Energies* **2022**, *15*, 5792.

39.   Clift, R., Grace, J.R., Weber, M.E. *Bubbles, Drops, and Particles*, Academic Press: New York, San Francisco, London, 1978.

40. Kutateladze, S.S., Malenkov, I.G. Experimental investigation of the analogy between the process of boiling and bubbling. *J. Appl. Mech. Tech. Phys.* **1966**, *7* (2) 97–99.

41. Rohsenow, W.M., Griffith, P. Correlation of maximum heat transfer data for boiling of saturated liquids. *Chem. Eng. Prog. Symp. Ser.* **1955**, *52*, 47–49.

42. Guan, C.-K., Klausner, J. F., Mei R. A new mechanistic model for pool boiling CHF on horizontal surfaces. *Int. J. Heat Mass Transfer* **2011**, *54*, 3960–3969.

43. Reyes, R., Wayner, J.P.C. An adsorption model for the superheat at the critical heat flux. *J. Heat Transfer* **1995**, *117*, 779–782.